Journal of Materials Chemistry A

ROYAL SOCIETY OF CHEMISTRY

PAPER

View Article Online
View Journal | View Issue

Check for updates

Cite this: *J. Mater. Chem. A*, 2024, **12**, 20278

A highly salt concentrated ethylene carbonate-based self-standing copolymer electrolyte for solid-state lithium metal batteries†

Nantapat Soontornnon, [a] Kento Kimura [b] and Yoichi Tominaga *[a]

Received 22nd May 2024
Accepted 24th June 2024

DOI: 10.1039/d4ta03543g

rsc.li/materials-a

CO_2-derived aliphatic polycarbonate-based solid polymer electrolytes (SPEs) with high Li salt concentrations promise notable electrochemical properties for solid-state lithium metal batteries (SSLMBs). However, adequate mechanical properties of these electrolytes for long-cycle-life batteries have rarely been obtained. In this work, we achieved long cycling of SSLMBs utilizing an electrolyte based on CO_2-derived crosslinked random poly(ethylene carbonate-*co*-ethylene oxide-*co*-allyl glycidyl ether) (CP). The CP with as high as 29% crosslinking unit ratio (CP_{29}) dissolving a high concentration of LiFSI can be obtained as a mechanically stable self-standing membrane and functions as an efficient electrolyte with a reasonable ionic conductivity. Remarkably, a Li//$LiFePO_4$ SSLMB with the electrolyte as the self-standing separator enabled rechargeable operation for 400 cycles at 40 °C, with a coulombic efficiency of more than 99.5%. This work will pave the way to realize long-cycle-life SSLMBs with highly concentrated crosslinked polymer electrolytes in the future.

Introduction

Solid-state lithium metal batteries (SSLMBs) have gained ever-increasing attention due to their improved safety as well as their high energy density in comparison with the organic liquid-based counterparts.[1–3] In the polymer-based SSLMBs, conventional liquid electrolytes are substituted with solid polymer electrolytes (SPEs), which impart thermal stability and good processability.[4,5] In 1973, Wright *et al.* first reported the ion-conductive properties of poly(ethylene oxide) (PEO)–metal salt complexes.[6] Since the discovery of PEO-based SPEs, various studies have been conducted to apply PEO-based SPEs as an electrolyte in battery systems due to their low glass transition temperature (T_g), which is favorable for fast ionic conduction mainly occurring in the amorphous region.[7,8] Unfortunately, an increase in salt concentration leads to an increase in T_g due to the strong and stable complex between Li^+ and the ether unit, obstructing the motion of the polymer chains, which inhibits ion migration.[9–11]

Aliphatic polycarbonates can be derived from the copolymerization of epoxides and CO_2. The synthetic method was first reported by Inoue and co-workers in 1968.[12] Motivated by the concept of CO_2 utilization, our group initiated studies to prepare SPEs from poly(ethylene carbonate) (PEC), one of the CO_2-derived aliphatic polycarbonates. The PEC-SPEs containing imide-type Li salts such as LiTFSI and LiFSI were found to have intriguing electrochemical properties. An increase in salt concentration of the PEC-based electrolytes results in better ionic conductivity with increased carrier ions and lowered T_g, unlike the PEO system.[13] Moreover, the PEC-SPEs were found to give rise to a high lithium transference number (t_{Li+}) with high oxidation stability and prevention of Al corrosion thanks to their highly concentrated nature.[14–16] Despite the electrolyte properties being improved at high salt concentrations, their low ionic conductivity issues remain compared to the PEO system. To utilize the advantages of polyether- and polycarbonate-based SPEs, poly(ethylene carbonate-*co*-ethylene oxide) P(EC/EO) has been synthesized and evaluated in our previous study. The results revealed that the highly concentrated P(EC/EO) electrolytes exhibit excellent ionic conductivity, which is higher than that of the PEC-based electrolyte at the equivalent salt concentration.[17] However, the presence of the soft EO segment and the excessive plasticizing effect of a high content of salt cause the P(EC/EO)-based electrolytes to be soft and resin-like materials, which are not self-standing and difficult to handle. The poor mechanical properties of the P(EC/EO)-based SPEs thus remained an issue to address.

To enhance the mechanical properties of non-polyether SPEs, many strategies, such as block copolymers,[18,19] reinforcement by ceramic fillers,[20,21] and crosslinking,[22–24] have been attempted. Our group also attempted to improve the

[a]*Graduate School of Bio-Applications and Systems Engineering (BASE), Tokyo University of Agriculture and Technology, 2-24-16 Nakacho, Koganei, Tokyo 184-8588, Japan. E-mail: ytominag@cc.tuat.ac.jp*

[b]*Department of Applied Chemistry, Graduate School of Engineering, Tokyo University of Agriculture and Technology, 2-24-16 Nakacho, Koganei, Tokyo 184-8588, Japan*

† Electronic supplementary information (ESI) available: Additional figures and tables for physicochemical and electrochemical properties, and photographic images of crosslinked copolymers. See DOI: https://doi.org/10.1039/d4ta03543g

mechanical properties of P(EC/EO)-based SPEs by introducing an allyl glycidyl ether (AGE) unit to obtain crosslinked random poly(ethylene carbonate-*co*-ethylene oxide-*co*-allyl glycidyl ether) (CP).[25] This crosslinked copolymer exhibited increased mechanical strength for better use in SPE and cathode binders.[26] Moreover, the CP electrolytes filled with TiO_2 were proved to enhance mechanical and ion-conductive properties, although long-cycle-life SSLMBs are yet to be obtained.[27] Crosslinking has also been commonly studied as a strategy to enhance the mechanical stability of the polyether-based SPE system, although the crosslinked polyether structures have been found to limit the salt dissolving power, particularly at high salt concentrations.[23,28–32] Therefore, the mechanically stable crosslinked copolymer-based SPE with high salt concentration should be an interesting novel concept to be explored.

Herein, we report the realization of a mechanically stable and self-standing highly concentrated crosslinked polymer electrolyte (CP-SPE) based on poly(ethylene carbonate-*co*-ethylene oxide-*co*-allyl glycidyl ether) (P(EC/EO/AGE)). The mechanically stable and highly concentrated CP-SPE was obtained by carefully optimizing the balance between the EC/EO/AGE unit ratio and Li salt concentration. Furthermore, we found that the short ether structure of AGE serves as the ion solvating unit to facilitate the salt dissociation at high salt concentrations together with the existence of the carbonyl group in the main chain. The ability of the CP-SPE to function as an electrolyte for long-cycle-life SSLMBs is finally evidenced by evaluation of mechanical, thermal, and electrochemical properties and charge/discharge testing of a prototype lithium metal cell.

Experimental

Chemicals

Ethylene oxide (EO, Air Water Inc., >99.9%, Osaka, Japan), carbon dioxide (CO_2, Taiyo Nippon Sanso, Japan, >99.99%), allyl glycidyl ether (AGE, TCI Co., Tokyo, Japan), lithium bis(fluorosulfonyl) mide (LiFSI, battery-grade, Kishida Chemical Co., Osaka, Japan), 1.45 wt% carbon-coated $LiFePO_4$ (LFP, Gelon Lib Group Co., Ltd, China), poly(vinylidene fluoride) (PVdF, Solef 5130, M_w = 1 000 000 to 1 100 000, Solvay Co., Belgium), acetylene black (AB, Denka Black®, Denka Co., Tokyo, Japan), poly(ethylene oxide) (PEO, M_w = 100 000, Thermo Scientific, Inc., Massachusetts, USA), *N*-methyl pyrrolidone (NMP, >99.5%, Kanto Chemical Co., Tokyo, Japan), acetonitrile (AN, >99.5%, dehydrated, Kanto Chemical Co., Tokyo, Japan), chloroform ($CHCl_3$, >99%, Kanto Chemical Co., Tokyo, Japan), hexane (C_6H_{14}, >96%, Kanto Chemical Co., Tokyo, Japan), methanol (CH_3OH, >99.8%, Kanto Chemical Co., Tokyo, Japan), zinc chloride ($ZnCl_2$, Hayashi Pure Chemical Ind., Ltd, Osaka, Japan), *tert*-butyl alcohol ($C_4H_{10}O$, >99%, TCI Co., Tokyo, Japan), and acetone (CH_3COCH_3, >99.5%, Kanto Chemical Co., Tokyo, Japan) were used as received. 2,2′-Azobisisobutyronitrile (AIBN, TCI Co., Tokyo, Japan) was purified by recrystallization with methanol before use. Poly(ethylene carbonate) (PEC, QPAC25, Empower Materials Ltd, New Castle, USA) was dissolved in acetonitrile and purified by pouring into excess methanol. The purified PEC was dried under vacuum at 60 °C for 48 h before use. Potassium hexacyanocobaltate(III) (crystalline $K_3[Co(CN)_6]$, >90%, Alfa Aesar, Massachusetts, USA), was purified twice by recrystallization in deionized water before use.

Synthesis of a double-metal cyanide (DMC) catalyst

A double-metal cyanide (DMC) catalyst was synthesized following the previous study.[17,33] Purified $K_3[Co(CN)_6]$ of 1.33 g was dissolved in 20 mL of deionized water and added dropwise into a $ZnCl_2$ solution (11.42 g of $ZnCl_2$ in 60 mL of deionized water and 30 mL of *tert*-butyl alcohol) under stirring for 45 min. Then, the mixed solution was stirred further for 60 min. The resulting white suspension was centrifuged at 10 000 rpm. Afterwards, the white solid was resuspended by stirring in a solution (*tert*-butyl alcohol/water = 50/50 by volume) for 30 min. The resulting suspension was precipitated by centrifuging again. The identical suspension/centrifugation process was repeated by gradually increasing the portion of *tert*-butyl alcohol against water (60/40, 70/30, 80/20, and 100/0). Finally, the obtained white solid was dried at 50 °C for 48 h. The chemical structure of the DMC catalyst can be found in previous study.[34]

Synthesis of P(EC/EO/AGE)

EO, AGE, and the DMC catalyst (0.001 g per 1 mL of EO + AGE) were introduced into a 100 mL autoclave (Taiatsu Techno Co.) with a magnetic stirrer. The EO : AGE (mol : mol) ratio was varied, as described in Table 1. Afterwards, 4 MPa of CO_2 was injected into the autoclave. In all processes, the exposure of the materials to the oxygen and moisture in the atmosphere was avoided by utilizing an Ar-vacuum line. The reaction was carried out at 60 °C for 20 h with a stirring speed of 600 rpm. The obtained copolymer was dissolved in chloroform and was purified by pouring the solution into excess MeOH : hexane with 2 to 3 drops of 1 M HCl(aq). This purification procedure was repeated 3 times. The purified copolymer was dried under vacuum at 60 °C for 48 h.

Synthesis of P(EC/EO)

P(EC/EO) was synthesized from EO as a monomer with a DMC catalyst (0.001 g per 1 mL of EO). The CO_2 pressure, temperature, reaction time, and purification procedure were identical to those for the synthesis of P(EC/EO/AGE).

Preparation of crosslinked P(EC/EO/AGE) (CP)

The obtained neat copolymer P(EC/EO/AGE) was weighed in a 30 mL bottle with 3 wt% of AIBN. The substances were

Table 1 Starting monomer ratios and results of copolymerization of 4 MPa CO_2 with EO and AGE using the DMC catalyst (at 60 °C for 20 h)

Copolymer	EO : AGE (mol)	Monomer unit (%)			M_n	M_w	PDI
		EC	EO	AGE			
$Neat_8$	10 : 1	60	32	8	1.3×10^5	3.8×10^5	2.9
$Neat_{14}$	5 : 1	58	28	14	1.6×10^5	4.2×10^5	2.6
$Neat_{23}$	3 : 1	54	23	23	5.1×10^4	1.3×10^5	2.6
$Neat_{29}$	2 : 1	52	19	29	6.2×10^4	2.2×10^5	3.6

dissolved in acetonitrile and blended using a planetary centrifugal mixer ARE-310 (THINKY, Tokyo, Japan) with a mixing speed of 2000 rpm for 20 min at room temperature. The solution was poured into a 50 mL poly(propylene) (PP) bottle in an Ar-filled glovebox. The crosslinking reaction was conducted at 60 °C for 48 h under reduced pressure. Finally, the solution was dried under vacuum at 60 °C for 48 h.

Preparation of solid polymer electrolytes (SPEs)

The obtained neat copolymer P(EC/EO/AGE) was weighed in a 30 mL bottle with various concentrations of LiFSI (x mol%: $[Li^+]/[EC + EO + AGE\ units] \times 100 = x$). Then, 3 wt% of AIBN with respect to the copolymer was introduced. All substances were dissolved in acetonitrile. Afterwards, the solutions were blended using a planetary centrifugal mixer with a mixing speed of 2000 rpm for 20 min at room temperature. The crosslinking process was carried out at 60 °C for 48 h under reduced pressure. Finally, the resulting solution was dried under Ar circulation at 60 °C for 24 h and under vacuum with a glass-tube oven at 60 °C for 48 h. For SPEs of reference polymers, the polymer and desired concentration of LiFSI (x mol%: $[Li^+]/[EO\ unit] \times 100 = x$ for PEO, $[Li^+]/[EC\ unit] \times 100 = x$ for PEC, and $[Li^+]/[EC + EO\ units] \times 100 = x$ for P(EC/EO)) were dissolved in acetonitrile in a 30 mL bottle. The solutions were blended using the same procedure as for the CP-SPE. Finally, the solutions were cast on a PTFE Petri dish and dried under Ar circulation at 60 °C for 24 h and under vacuum using a glass-tube oven at 60 °C for 48 h. The residual solvent of SPEs was estimated through ^{1}H NMR using a JNM-ECX400 spectrometer (JEOL Co. Ltd, Tokyo, Japan) by swelling the recorded amount of SPE samples (approximately 0.01 g) into $CDCl_3$ solvent for 24 h before the measurement. A constant weight of acetone (0.1 g) was added to the sample in the NMR tube as the reference for the calculation of the weight of residual solvent.

Preparation of the cathode

A composite cathode was made using the carbon-coated LFP with acetylene black (AB) as a conductive agent and PVdF as a binder in a weight ratio of LFP : AB : PVdF = 80 : 10 : 10. The components were mixed in NMP solvent using a planetary centrifugal mixer with a mixing speed of 2000 rpm for 20 min at room temperature to obtain a homogeneous slurry. Afterwards, the slurry was cast on a 20 μm-thick Al foil using a film applicator (Doctor blade No.15593, Yasuda Seiki, Hyogo, Japan) with a thickness of 4 mils (1 mil = 25.4 μm). The cast cathode was dried at 70 °C under vacuum for 24 h. Finally, the dried cathode was pressed at 70 °C with 10 MPa for 30 min and cut into a circle shape. The obtained cathode was 60 μm thick, excluding the Al foil layer.

Physicochemical, thermal, and mechanical characterization studies

The chemical structure of the obtained copolymers has been confirmed by ^{1}H NMR measurement using a JNM-ECX400 spectrometer. The neat copolymer was dissolved in $CDCl_3$. To investigate the molecular weight and polydispersity index (PDI) of neat copolymers by size exclusion chromatography (SEC), they were dissolved in chloroform and examined using an HLC-8320 GPC EcoSEC (TOSOH Co., Tokyo, Japan). To study the thermal properties of CPs and their electrolytes, differential scanning calorimetry (DSC) and thermogravimetric analysis (TGA) were employed to investigate the glass transition and degradation temperature. DSC was performed using a DSC7020 (Hitachi High- Tech Co., Tokyo, Japan) in the temperature range of −80 to 80 °C at a heating rate of 10 °C min^{-1} under N_2 gas flow of 40 mL min^{-1}. The TGA was carried out using a TG/DTA 7200 (Hitachi High-Tech Co.) in the temperature range of 30 to 500 °C at a heating rate of 10 °C min^{-1} under N_2 gas flow of 100 mL min^{-1}. Fourier-transform infrared spectroscopy (FT-IR) was conducted using an FT-IR-4100 (Jasco Co., Tokyo, Japan) equipped with an ATR unit (ZnSe lens) in the wavenumber range from 700 to 4000 cm^{-1} at a resolution of 4 cm^{-1}. The mechanical properties of the CPs were tested using a tensile tester EZ-LX equipped with a 50 N load cell (Shimadzu Co., Kyoto, Japan), while a small tensile tester OZ502 placed in an Ar-filled glovebox equipped with a 50 N load cell (Sentec Co., Osaka, Japan) was used for the CP_{29}-SPEs. Both tests were performed at a stretching speed of 10 mm min^{-1} at room temperature. Five measurements were conducted for the tensile test of each sample; a result that represents the average performance is selected to report in the text.

Electrochemical characterization

Symmetrical electrochemical cells with stainless steel as a blocking electrode (SS/SPE/SS) separated by a PTFE spacer were prepared to investigate the ionic conductivity of SPEs by potentiostatic electrochemical impedance spectroscopy (EIS). The cells were kept at 60 °C for 16 h for stabilization prior to the measurement. The measurements were performed within a frequency range of 10^6 to 10^2 Hz at an amplitude of 30 mV using a potentiostat/galvanostat SP-150 (Bio-Logic Co., Seyssinet-Pariset, France), while decreasing the temperature from 80 to 30 °C at 10 °C intervals. The ionic conductivity was determined by evaluating the bulk resistance. All processes were carried out in an Ar-filled glovebox. The oxidative stability of SPEs was investigated by linear sweep voltammetry (LSV) using the potentiostat/galvanostat SP-150 at a scanning rate of 1 mV s^{-1}. The cell configuration of LSV comprised a lithium metal sheet (lithium metal (Li), Honjo Metal Co., Osaka, Japan) as the counter/reference electrode and a stainless-steel disk (SS) as the working electrode (Li/SPE/SS) separated by a 150 μm-thick polyimide film (the center of the film was punched out into $\varphi = 6$ mm). The cells were kept at 40 °C for 16 h to stabilize the interfacial contact of the Li/SPE before the measurement. CR2032 coin cells (CR2032, Hohsen Co., Tokyo, Japan) for the battery test were assembled with the LFP cathode. The SPE membrane was placed on the cathode. Then, the Li metal foil anode was placed on the SPE. The cells were assembled in an Ar-filled glovebox. The galvanostatic charge/discharge test was carried out using an HJ1001SM8A battery test system (Hokuto Denko Co., Tokyo, Japan) at a current rate of $C/10$ ($1C = 160$ mA g^{-1}) at 40 °C within a voltage range of 2.5–3.8 V. All cells were kept at the measuring temperature for 24 h before beginning

measurements. EIS measurements of the cells during the battery cycling were conducted using a potentiostat/galvanostat VSP-300 (Bio-Logic) within a frequency range of 3×10^6 to 10^{-1} Hz at an amplitude of 30 mV. The impedance spectra were fitted with the equivalent circuit through the Z-fit of the EC-Lab software.

Results and discussion

Chemical properties of CPs

To look into the effect of the crosslinking unit ratio on the properties of the CPs and the CP-SPEs based on them, random P(EC/EO/AGE) copolymers were synthesized with varied preparation ratios of the AGE monomer. The copolymers having double bonds to crosslink were synthesized by copolymerization of CO_2, EO, and AGE with a double-metal cyanide (DMC) catalyst (Scheme S1†). The copolymerization of CO_2 and epoxide species typically gives a certain ratio of carbonate and ether linkages of copolymer, depending on the polymerization conditions and catalysts. The DMC catalyst was selected in this work because it is known for its versatility in controlling the carbonate/ether unit ratio by varying reaction conditions such as CO_2 pressure and temperature.[35,36]

^{1}H NMR confirmed the chemical structures of the obtained copolymers before crosslinking (Neat$_x$, where x represents the amount of the AGE unit), as shown in Fig. 1. The ^{1}H NMR signals are assigned as follows. The peaks at around 4.3 ppm are the CH_2 groups in the (a) carbonate–carbonate chain, which is similar to the peak of PEC in Fig. S1,† and (b) carbonate–ether chain (carbonate side).[25] The peaks at around 3.8 ppm are determined as the CH_2 groups in the (c) ether–carbonate chain (ether side) and (d) ether–ether chain.[25] The characteristic peaks of the carbonate–ether chain (b and c) shown above were similar to the peaks of P(EC/EO) in Fig. S2.† Compared to the spectrum of P(EC/EO), the spectrum of P(EC/EO/AGE) copolymer exhibits the characteristic peaks of the AGE unit. The peaks at 4.9 ppm (i) and 3.9 ppm (j) are assigned to the CH groups adjacent to the carbonate linkage and the ether linkage in the AGE unit backbone, respectively.[37] The overlapping peaks at around 3.5 ppm (k/k′/k″) are the CH_2 adjacent to the CH group. The peak at around 4.0 ppm (h/h′) is assigned to CH_2 of the allyl group adjacent to the ether linkage in the side chain.[37] The peaks at 5.9 ppm (e/e′) and 5.2 ppm (f/f′) are the double bonds of the methylene side and the terminal side, respectively.[25,37] To calculate the EC : EO : AGE molar ratios, we utilized the integral peak areas of the characteristic ^{1}H NMR signals of EC, EO, and AGE units (Fig. S3†). The monomer ratio was calculated from the equation.

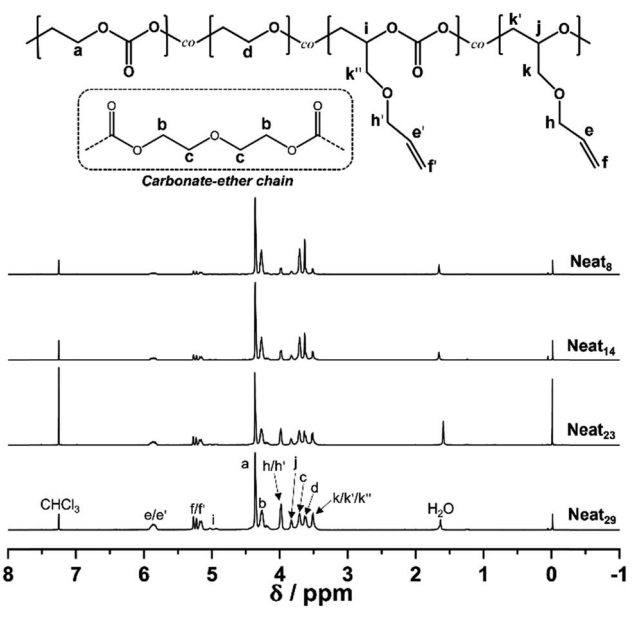

Fig. 1 ^{1}H NMR spectra of P(EC/EO/AGE) copolymers before crosslinking.

$$\mathrm{EC : EO : AGE} = \frac{I_{a+b}}{H_{a+b}} : \frac{I_{c+d}}{H_{c+d}} : \frac{I_e}{H_e}$$

where I and H are the integral area of each peak and the number of protons for each monomer unit, respectively. The unit ratios calculated using the equation are summarized in Table 1. All the obtained neat P(EC/EO/AGE) copolymers had average molecular weight (M_w) values of more than 100 000 with PDIs around 2.5 to 3.5, as also shown in Table 1.

Mechanical and thermal properties of CPs

The occurrence of crosslinking was confirmed for all the obtained CPs by the disappearance of the allyl group peak at 1648 cm^{-1} (ref. 38) in FT-IR (Fig. S4†). A tensile test was employed to compare the mechanical strength of the obtained CPs. The stress–strain curves are reported in Fig. 2(a). The Young's modulus values were estimated from the slope in the initial linear region of the stress–strain curves, as summarized in Fig. 2(b). Fig. 2(a) shows that the increase in the AGE ratio gives an increasing trend of mechanical stress at the identical strain values with reduced elongation at break, where the stress at break reaches a maximum of 2.5 MPa. Fig. 2(b) also shows an upward trend of Young's modulus to give a value of 23.5 MPa for CP_{29}. The observations reveal that the presence of dense crosslinking units provides the CPs with more elastic and brittle nature. The TGA curves in Fig. 2(c) give evidence that the decomposition temperature at 5 wt% loss (T_{d5}) slightly increased with increasing AGE unit to reach the highest T_{d5} of 260 °C at CP_{29} (Table S1† summarises T_{d5} values). This is probably due to the decrease in the EC linkage ratio, which should inhibit the back-biting reaction that occurs starting from the polymer chain ends with carbonate linkages.[39–41] Furthermore, DSC (Fig. 2(d)) shows a decreasing trend of the T_g with increasing AGE ratio, which is probably attributed to the increased ether side chains of the AGE unit to enhance the segmental motion of polymer chains.

Ion-conductive properties of CP-SPEs

Afterwards, the CP-based solid polymer electrolytes (CP-SPEs) with various LiFSI concentrations were prepared by simply adding LiFSI into the reacting solution of the neat copolymers

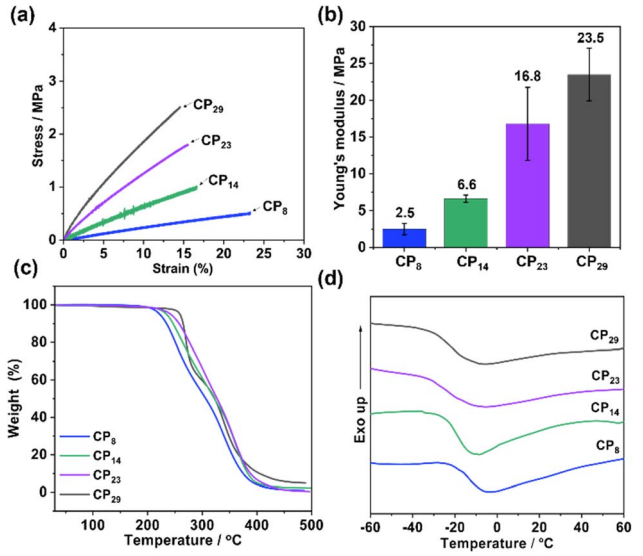

Fig. 2 (a) Tensile stress–strain curves, (b) Young's modulus values (error bar: standard deviation), (c) TGA thermograms, and (d) DSC curves of the CPs.

with the AIBN initiator and evaluated as battery electrolytes. Fig. 3(a) summarizes the salt concentration dependence of the ionic conductivity at 40 °C for all the CP-SPEs. The ionic conductivity of the electrolytes at 120 mol% of LiFSI was also compared in the form of the Arrhenius plot in Fig. 3(b). These results reveal that the CP-SPEs exhibit similar trends, showing peaks of ionic conductivity at certain LiFSI concentrations. We assume that this behavior reflects the balance between the EC-like and EO-like salt concentration dependence behavior. It is known that the salt addition to PEO tends to decrease the conductivity due to the reduced segmental motion by the interaction between Li ions and ether chains, while PEC shows an opposite trend of increase in conductivity due to a superior effect of plasticization by the salt addition.[11,13,42] The CP_{23}-SPE provides high ionic conductivity in the relatively low salt concentration regime to reach a maximum of 5.7×10^{-5} S cm^{-1} at 40 °C at 120 mol%. Nevertheless, this electrolyte could not be obtained as a self-standing membrane, but rather a soft and sticky resin-like material, which could not be subjected to the tensile test. In contrast, the CP_{29}-SPE displays an increasing

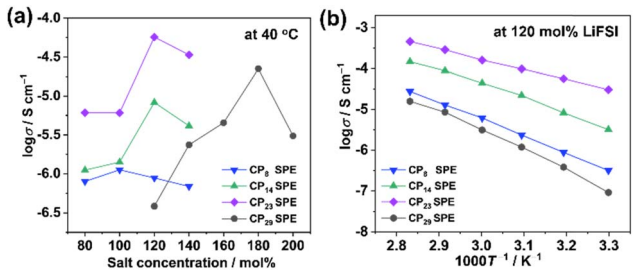

Fig. 3 (a) Salt concentration dependence of the ionic conductivity at 40 °C for CP-SPEs and (b) temperature dependence of the ionic conductivity for CP-SPEs at 120 mol% of LiFSI.

ionic conductivity trend from 120 to 180 mol%, where tough and flexible membranes are successfully obtained. The photographs of CP_{29} and CP_{29}-SPE are shown in Fig. S5† and Fig. 4(b–d), respectively. We assume that the significance of the EC-like behavior of the CP_{29}-SPE, which enabled the reasonable ionic conductivity at the LiFSI concentration of as high as 180 mol%, relates to the highest EC/EO unit ratio. To compare with ether-based SPEs, most evaluated species in the field, PEO-LiFSI 5 mol%, which showed the highest ionic conductivity in our previous studies,[17,43] was chosen for direct comparison with CP_{29}-SPEs in Fig. S6.† The result shows that the CP_{29}-SPEs had the ionic conductivity close to that of the PEO electrolyte at high LiFSI concentration around 180 mol% in the high temperature range with a merit of higher conductivity at ambient temperature range due to their amorphous nature. Based on these results, CP_{29}-based electrolytes are hereafter chosen as the highly concentrated crosslinked electrolyte system to study the physicochemical, mechanical, and electrochemical properties in detail.

Details of CP_{29} and CP_{29}-SPEs

Having chosen the CP_{29} as the most suitable matrix, the properties of CP_{29} and CP_{29}-SPEs are further studied in detail. In this study, PEC- and P(EC/EO)-based SPEs are used as the reference materials to compare with the CP_{29}-SPEs. The comparison between DSC curves and T_g values of PEC and P(EC/EO) (Fig. S7† and Table 2) suggests that introducing EO units significantly reduces T_g due to the facilitated segmental motion by ether linkages. Interestingly, the T_g of CP_{29} was further lowered from −22 °C to −31 °C compared to the P(EC/EO). We assume that the segmental motion was further promoted by the ether linkages in the side chains of the AGE unit. The TGA thermograms and T_{d5} values (Fig. S8† and Table 2) also give evidence of the thermal stability of CP_{29} improved by the presence of both EO and AGE units, where the T_{d5} reaches 260 °C. As mentioned above, the aliphatic polycarbonate decomposes *via* the back-biting mechanism.[39,40] The increased ratio of the non-EC linkage is attributed to the enhanced thermal decomposition temperature.

FT-IR spectra in Fig. S9† confirmed the crosslinking reaction even with the presence of concentrated LiFSI in the reacting solution, where the peak of the allyl group at 1648 cm^{-1} (ref. 38) vanished. ^{1}H NMR confirmed that the residual solvent (acetonitrile, AN) of CP_{29}-SPEs was estimated to be less than 2 wt% (see the detailed procedure of the estimation described in Fig. S10†), which may have negligible impact on this study. DSC

Table 2 Chemical and thermal properties of PEC, P(EC/EO), and CP_{29}

	Monomer unit (%)						
Polymer	EC	EO	AGE	M_n	M_w	T_g (°C)	T_{d5} (°C)
PEC	99	<1%	—	3.5×10^4	1.2×10^5	17	195
P(EC/EO)	56	44	—	7.0×10^4	1.5×10^5	−22	233
CP_{29}	52	19	29	6.2×10^4	2.2×10^5	−31	260

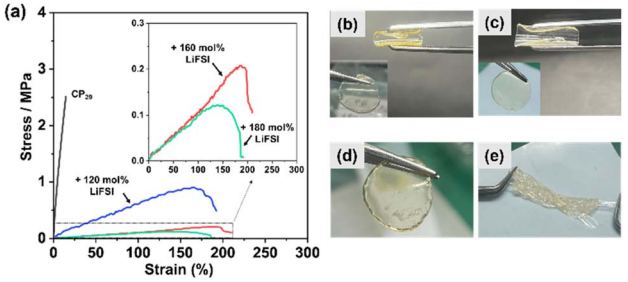

Fig. 4 (a) Tensile stress–strain curves of CP_{29} and CP_{29}-based SPEs. Photographs of CP_{29}-SPEs at LiFSI concentration of (b) 120 mol%, (c) 160 mol%, and (d) 180 mol% (∅ = 14 mm). (e) Photograph of P(EC/EO)-180 mol% LiFSI.

was employed to characterize the T_g of CP_{29}-based electrolytes at the different salt concentrations, as shown in Fig. S11(a).† The T_g data are given in Table S2.† The increase in salt concentration gave rise to a decrease in T_g to reach −55 °C at 180 mol%, which reflects the EC-like behavior of the CP_{29}, as discussed above. TGA in Fig. S11(b)† was utilized to analyze the decomposing temperature. The T_{d5} data are also summarized in Table S2.† Although the results showed a decrease in decomposing temperature with the addition of LiFSI, T_{d5} values around 150 °C are demonstrated for the CP_{29}-based electrolytes. Besides, the TGA curves also showed a certain increase in the final residual mass (%) with increasing salt concentration, indicating the residual product from the decomposition of lithium salt, which has also been found in previous studies.[44–46]

The stress–strain curves and Young's modulus values of the CP_{29}-based electrolytes are reported in Fig. 4(a) and Table S2,† respectively. The CP_{29}-120 mol% LiFSI had the highest Young's modulus of 0.8 MPa and was reduced upon the increases in salt concentration. The elongation at break was also reduced by the change of salt concentration from 160 to 180 mol%. Photographs of CP-SPEs in Fig. 4(b–d) revealed obviously that the CP_{29}-SPEs exhibit a self-standing membrane while the P(EC/EO)-180 mol% LiFSI SPE (Fig. 4(e)) is soft as a resin-like material and could not be subjected to tensile-test. These results suggest that the salt concentration needs to be carefully optimized to realize good mechanical and electrochemical properties simultaneously.

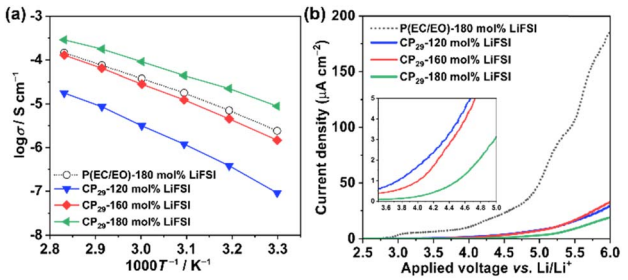

Fig. 5 (a) Temperature dependence of the ionic conductivity and (b) LSV curves at 40 °C with a scanning rate of 1 mV s^{-1} for CP_{29}-based SPEs at various LiFSI concentrations and P(EC/EO)-180 mol% LiFSI.

The Arrhenius plot of ionic conductivity in Fig. 5(a) compares the ionic conductivities of CP_{29}-SPEs and the P(EC/EO)-based SPE. It is worth noting that the ionic conductivity of the CP_{29}-180 mol% LiFSI electrolyte is higher than that of the P(EC/EO)-based SPE to reach 2.2×10^{-5} S cm^{-1} at 40 °C. This agrees with the decreased T_g of the CP_{29} when compared with P(EC/EO). The ionic conductivity of the CP_{29}-160 mol% LiFSI electrolyte was measured to be 4.5×10^{-6} S cm^{-1} at 40 °C and is lower than that of the 180 mol% electrolyte, although it has the benefit of greater mechanical properties. We also assume that the existence of ether linkages in the crosslinking chains of the AGE unit might enhance the ion dissociation and, thus ionic conduction, which will be discussed by employing an FT-IR study in the following section. To achieve a solid electrolyte for practical use in batteries, the electrolytes need to be electrochemically stable with the high voltage operation of the battery cathode. Thus, the oxidative stability of the CP_{29}-SPE was investigated by LSV as displayed in Fig. 5(b). The results show that all CP_{29}-SPEs have oxidative stability above 4 V *vs.* Li/Li^+ (the voltage at 2 μA cm^{-2}). It is also noteworthy that the increase in LiFSI concentration gives rise to a greater oxidative stability. This is probably due to the highly aggregated structure of Li^+ and imide-type anions, which has been reported to improve the oxidation stability of the solvent with reduced electron densities.[47,48] Furthermore, the LSV data also confirm that the CP_{29}-SPEs had oxidation stability higher than that of P(EC/EO)-180 mol% LiFSI. A study has found that the oxidation of EO chains in the PEO/LiTFSI electrolyte occurs at a low voltage of around 3.2 V *vs.* Li/Li^+ due to the deprotonation of the –OH group at the polymer chain end by the imide-type anion ($TFSI^-$), which results in the formation of HTFSI.[49] A further increase in the voltage up to around 3.5 V *vs.* Li/Li^+ causes the EO main chain to be oxidized to form some alcohol products.[49] In our LSV result, the P(EC/EO) electrolyte shows similar oxidation steps that occur at around 3.0 and 3.7 V *vs.* Li/Li^+. Therefore, the improved oxidation stability of the CP_{29}-SPE highlights that the AGE crosslinking unit probably has an effect to suppress these oxidation steps of EO chains.

FT-IR spectroscopy

To understand the interaction between the dissolved ions and polymer chain in the different polymer hosts, the FT-IR study was conducted as shown in Fig. 6. Fig. 6(a) illustrates the FT-IR spectra of the carbonate (C=O) stretching vibration mode ($\nu_{C=O}$) at the LiFSI concentration of 0 (original polymers), 10 and 180 mol%. All original polymers without the addition of salt show the characteristic peaks of $\nu_{C=O}$ at 1739, 1740, and 1744 cm^{-1} for PEC, P(EC/EO), and CP_{29} systems, respectively. The $\nu_{C=O}$ peak of CP_{29} is located in a significantly higher wavenumber than PEC and P(EC/EO). Our previous study has confirmed that a conformation change of the PEC chain from *gauche* to *trans*, which reflects a restriction of the intramolecular interaction between C=O and CH_2, leads to a higher wavenumber of the free C=O peak, with the support of density functional theory (DFT) calculations for the model oligomer.[16] Therefore, the shift of the $\nu_{C=O}$ peak of CP_{29} is probably because the presence of the

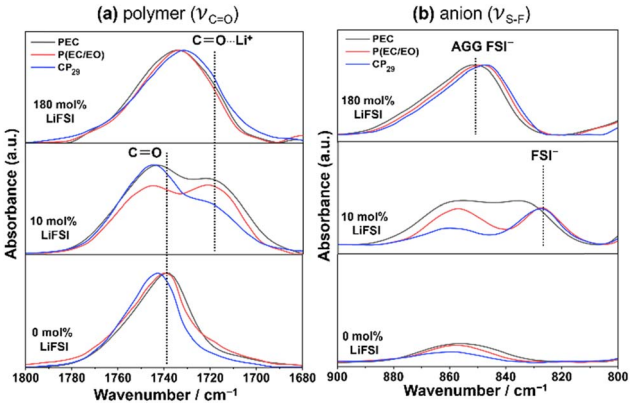

Fig. 6 FT-IR spectra of the neat polymer and the SPEs at 10 and 180 mol% LiFSI in the stretching vibration region of (a) C=O ($\nu_{C=O}$) of the polymers and (b) S–F (ν_{S-F}) of the FSI anion.

AGE unit somehow facilitates the carbonate conformation changes from *gauche* to *trans* by restricting the former.[27] To distinguish the peak positions of free C=O and C=O interacting with the Li cation (C=O···Li^+), the SPEs with 10 mol% of LiFSI were utilized. It was clear that the C=O···Li^+ peak appeared at approximately 1720 cm^{-1}[50] in these polymer systems. When 180 mol% of LiFSI was introduced into the neat polymers, the distinct $\nu_{C=O}$ peaks of free and interacting C=O at 10 mol% merge into a broad overlapped peak at around 1735, 1733, and 1730 cm^{-1} for PEC, P(EC/EO), and CP_{29}, respectively. Our previous study has also revealed that the C=O···Li^+ peak gradually shifts with increasing LiFSI concentration to a higher wavenumber from the initial 1720 cm^{-1} as the C=O···Li^+ interaction is reduced by the increasing contact between Li^+ and FSI^- ions (C=O···Li^{+}···FSI^-).[14,51] We suppose that the C=O···Li^+ peak is obscured by the contribution of free C=O due to the above weakening of the interaction, which leads to the shift to higher wavenumber. In the spectra of 180 mol% electrolytes, the CP_{29}-SPE shows the trend of the lowest wavenumber of the merged peak compared to the PEC- and P(EC/EO)-SPEs. The existence of ether linkages in the AGE crosslinking units may play a role in facilitating the ion dissociation, as discussed below.

To better understand the effect of ion solvation on the anion in the polymer system, Fig. 6(b) shows the stretching vibration of the S–F bond (ν_{S-F}) in the wavenumber 900–800 cm^{-1}. The addition of 10 mol% of LiFSI into the polymer hosts gives characteristic ν_{S-F} peaks at approximately 827 cm^{-1} for P(EC/EO) and CP_{29} electrolytes, while the peak was found at approximately 835 cm^{-1} for PEC. At 180 mol%, the ν_{S-F} peaks for the SPEs exhibit a dramatic shift to higher wavenumbers around 850 cm^{-1}. The peaks were at the lower wavenumber positions in the order of CP_{29}, P(EC/EO), and PEC electrolytes. A previous study has confirmed that the peak of aggregated FSI^- (AGG FSI^-) was distinct from the free FSI anion (FSI^-), which was found at the higher wavenumber in the dimethyl carbonate (DMC) electrolyte system.[52] The peak at a higher wavenumber of the PEC electrolyte represents the higher tendency to form AGGs, while P(EC/EO) and CP_{29}, which contain ether chains to form complex structures more strongly with Li ions, have a higher tendency to dissociate salt. It is also worth noting that the ν_{S-F} peak of CP_{29} is found at a slightly lower wavenumber at 180 mol%, which agrees with the lower wavenumber of the C=O···Li^+ ($\nu_{C=O}$) peak than that of the P(EC/EO). Given the higher EC/EO ratio of CP_{29} than that of P(EC/EO) used in this study (2.7 for CP_{29} and 1.3 for P(EC/EO), see Table 2), we suppose that the existence of ether linkages in the AGE crosslinking unit has an ability to facilitate the salt dissociation, which is advantageous to increase carrier ions and thus promote the ionic conduction, in our CP-SPE system.

Battery performance and electrochemical impedance of CP_{29}-SPEs

As the CP_{29}-180 mol% LiFSI electrolyte was confirmed to show the highest ionic conductivity, it was first selected as an electrolyte to test in a Li//LFP cell. The charge/discharge voltage profiles are shown in Fig. S12(a).† The results revealed that CP_{29}-180 mol% LiFSI gives the discharge capacity of 135 mA h g^{-1} at the first cycle with a sudden decrease of the capacity at the eighth cycle, as shown in Fig. S12(b).† Even though CP_{29}-180 mol% LiFSI provides the highest ionic conductivity, the low mechanical strength may result in the low stability of cycling. To achieve better charge/discharge cycling stability, CP_{29}-160 mol% LiFSI, which has both reasonable ionic conductivity and mechanical properties, was also chosen as an electrolyte to test. Fig. 7(a) presents the voltage profiles of the Li//LFP cell at 40 °C. Fig. 7(b) also exhibits the cycling performance of the cell. The obtained discharge capacity was approximately 58 mA h g^{-1} at the first cycle and then gradually increased to a maximum of 90 mA h g^{-1} at around the 20th cycle. After that, the discharge capacity was slightly reduced and stabilized at around 80 mA h g^{-1} after approximately 100 cycles. Although it is difficult to assign the exact phenomenon that originates this fluctuation, we assume that this was caused by mixed effects of an improved attachment of the SPE/LFP interface and a stabilization process of the solid electrolyte interphase (SEI) on the surface of both the Li anode and LFP cathode, as further discussed below. The result also suggests that coulombic efficiency (CE) remains consistently high, more than 99.5% after the 400th cycle, even though some cycles have fluctuations. The battery cycling test results confirm the clear potential of CP_{29}-160 mol% LiFSI as an electrolyte for long-cycle-life SSLMBs.

To look deep into the resistance behavior of the cell, electrochemical impedance spectroscopy (EIS) measurements were conducted before the cycling and after every 100 cycles, as summarized in Fig. 7(c). The plots were fitted using the equivalent circuit model illustrated in the figure. The fitting values are summarized in Table S3.† In this circuit model, R_1 denotes the bulk resistance, which reflects the conductivities of the CP_{29}-SPE.[53,54] Then, R_2 and R_3 indicate the charge-transfer resistance between the Li/SPE interface and the SPE/LFP interface, respectively.[55] Lastly, W is the Warburg impedance assigned to the effect of a diffusion-limited electrochemical process within the SPE/LFP area.[56] As a result of the fitting study, the cycle number evolution of R_1, R_2, and R_3 is

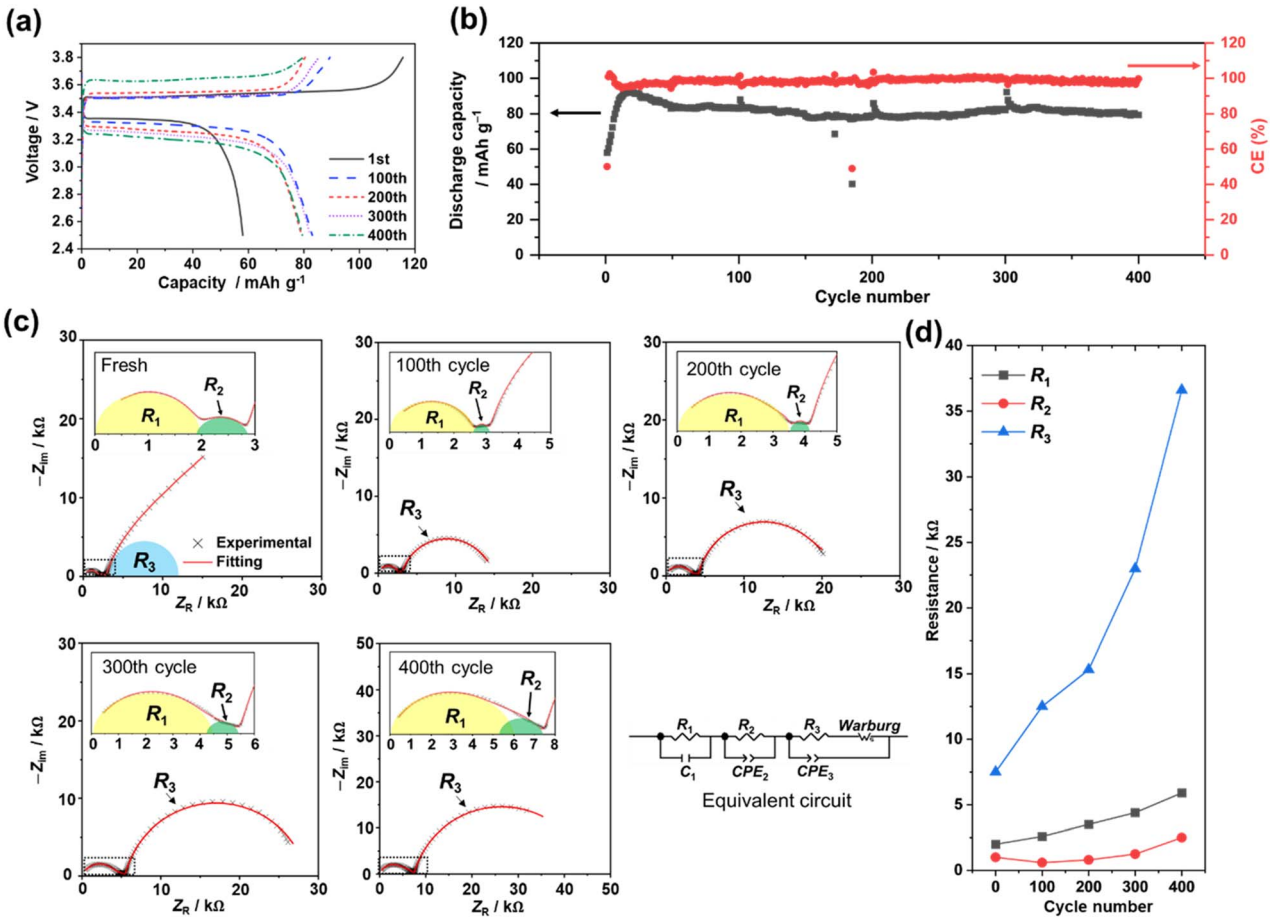

Fig. 7 (a) Voltage profiles of charge/discharge, (b) cycling performance, (c) Nyquist plot for fresh and after cycles with the fitting equivalent circuit model for EIS, and (d) cycle number evolution of the resistance of Li//LFP cells (cathode mass loading: 2.0 mg cm^{-2} of active materials) using CP_{29}-160 mol% LiFSI as an electrolyte at $C/10$ rate ($1C = 160$ mA g^{-1}) at 40 °C.

summarized in Fig. 7(d). The result confirmed that at the 100th cycle, the R_2 value was reduced compared to the fresh cell. This resistance reduction probably indicates that a good contact of the Li/SPE interface was built after the initial conditioning process, which might have led to an increase in the discharge capacity, as shown above. Nonetheless, the R_2 continuously increased after 200 cycles, which could be attributed to many origins, such as the thickening film layer of the Li/SPE interface and porous structures of Li after cycling.[57] R_1 also shows an increasing trend, possibly due to Li-salt degradation in the electrolyte.[58] Moreover, the R_3 value increased dramatically from 7.52 kΩ of the fresh cell to 36.58 kΩ of the cell at the 400th cycle. We suppose that the increase in R_3 indicates that the charge/discharge cycling causes a poor SPE/LFP interfacial contact, possibly due to the gradual deterioration of cathode material components.[59] These results suggest that obtaining more stable SPE/electrode interfacial resistances by optimizing the battery electrode components may provide more prolonged cycling beyond the current limit of 400 cycles. These prototype battery investigations confirm the clear potential of the highly concentrated crosslinked polymer-based electrolyte for long-cycle-life SSLMBs.

Conclusions

Crosslinked P(EC/EO/AGE) copolymers having various AGE crosslinking units were synthesized and evaluated as a polymer matrix for SPEs with high concentrations of LiFSI to enable long-cycle-life SSLMBs. Through comparative studies of the CPs and their electrolytes (CP-SPEs), the effect of the combination between the EC/EO/AGE unit ratio and LiFSI concentration was carefully studied to optimize. As a result, we found that the electrolyte with 29% AGE units and LiFSI at a concentration of as high as 160 mol% results in a reasonable ionic conductivity and favorable mechanical properties simultaneously. FT-IR results suggested that the ether side chain in the AGE unit serves as the salt solvating unit to aid salt dissociation and thus ionic conduction at high salt concentrations. The CP_{29}-160 mol% LiFSI electrolyte can be obtained as a flexible and self-standing membrane. Remarkably, galvanostatic charge/discharge testing of the Li//LFP cell employing the CP_{29}-160 mol% LiFSI electrolyte membrane as a self-standing separator exhibited rechargeable operation for up to 400 cycles at 40 °C with a sustaining coulombic efficiency of more than 99.5%. All results suggest that the highly concentrated crosslinked copolymer electrolyte has the potential as a new concept to enable

solid electrolytes with excellent electrochemical and mechanical properties to realize long-cycle-life solid-state lithium metal batteries in the future.

Data availability

The data supporting this article have been included as part of the ESI.†

Author contributions

The authors confirm contribution to the paper as follows: N. S. contributed to study conception and design, experimental design, data curation, investigation, and writing-original draft. K. K. contributed to supervision and writing-review and editing. Y. T. contributed to supervision, funding acquisition, study conception and design, and writing-review and editing.

Conflicts of interest

There are no conflicts to declare.

Acknowledgements

This work was supported financially by a Grant-in-Aid for Scientific Research (B) of JSPS KAKENHI (No. 23K23057) and Adaptable and Seamless Technology transfer Program through Target-driven R&D (A-STEP) of JST (No. JPMJTR22T2), Japan. This work was also supported partly by the Ministry of Education, Culture, Sports, Science and Technology (Monbukagakusho: MEXT) scholarship (No. 213354), Japan.

References

1 C. Zhang, Q. Hu, Y. Shen and W. Liu, *Adv. Energy Sustainability Res.*, 2022, **3**, 2100203.
2 J. Liu, H. Yuan, H. Liu, C. Z. Zhao, Y. Lu, X. B. Cheng, J. Q. Huang and Q. Zhang, *Adv. Energy Mater.*, 2021, **12**, 2100748.
3 M. Arrese-Igor, M. Martinez-Ibañez, E. Pavlenko, M. Forsyth, H. Zhu, M. Armand, F. Aguesse and P. López-Aranguren, *ACS Energy Lett.*, 2022, **7**, 1473–1480.
4 G. Xi, M. Xiao, S. Wang, D. Han, Y. Li and Y. Meng, *Adv. Funct. Mater.*, 2020, **31**, 2007598.
5 X. Zhao, C. Wang, H. Liu, Y. Liang and L. Z. Fan, *Batteries Supercaps*, 2023, **6**, e202200502.
6 D. E. Fenton, J. M. Parker and P. V. Wright, *Polymer*, 1973, **14**, 589.
7 Z. Xue, D. He and X. Xie, *J. Mater. Chem. A*, 2015, **3**, 19218–19253.
8 J. Mu, S. Liao, L. Shi, B. Su, F. Xu, Z. Guo, H. Li and F. Wei, *Polym. Chem.*, 2024, **15**, 473–499.
9 Y. G. Andreev, P. Lightfoot and P. G. Bruce, *Chem. Commun.*, 1996, 2169–2170.
10 M. Z. A. Munshi, B. B. Owens and S. Nguyen, *Polym. J.*, 1988, **20**, 597–602.
11 M. A. Ratner and D. F. Shriver, *Chem. Rev.*, 2002, **88**, 109–124.
12 S. Inoue, H. Koinuma and T. Tsuruta, *J. Polym. Sci. B Polym. Lett.*, 1969, **7**, 287–292.
13 Y. Tominaga, *Polym. J.*, 2016, **49**, 291–299.
14 K. Kimura, J. Motomatsu and Y. Tominaga, *J. Polym. Sci. B Polym. Phys.*, 2016, **54**, 2442–2447.
15 K. Kimura, M. Yajima and Y. Tominaga, *Electrochem. Commun.*, 2016, **66**, 46–48.
16 K. Kimura and Y. Tominaga, *ChemElectroChem*, 2018, **5**, 4008–4014.
17 T. Morioka, K. Nakano and Y. Tominaga, *Macromol. Rapid Commun.*, 2017, **38**, 1600652.
18 A. Bergfelt, M. J. Lacey, J. Hedman, C. Sangeland, D. Brandell and T. Bowden, *RSC Adv.*, 2018, **8**, 16716–16725.
19 B. Zhang, Y. Liu, X. Pan, J. Liu, K. Doyle-Davis, L. Sun, J. Liu, X. Jiao, J. Jie, H. Xie and X. Sun, *Nano Energy*, 2020, **72**, 104690.
20 F. P. Nkosi, M. Valvo, J. Mindemark, N. A. Dzulkurnain, G. Hernández, A. Mahun, S. Abbrent, J. Brus, L. Kobera and K. Edström, *ACS Appl. Energy Mater.*, 2021, **4**, 2531–2542.
21 Z. Li, H. Matsumoto and Y. Tominaga, *Polym. Adv. Technol.*, 2017, **29**, 820–824.
22 I. L. Johansson, D. Brandell and J. Mindemark, *Batteries Supercaps*, 2020, **3**, 527–533.
23 L. Meabe, T. V. Huynh, D. Mantione, L. Porcarelli, C. Li, L. A. O'Dell, H. Sardon, M. Armand, M. Forsyth and D. Mecerreyes, *Electrochim. Acta*, 2019, **302**, 414–421.
24 J. Mindemark, A. Sobkowiak, G. Oltean, D. Brandell and T. Gustafsson, *Electrochim. Acta*, 2017, **230**, 189–195.
25 N. Nishimura, J. Hashinokuchi and Y. Tominaga, *Macromol. Chem. Phys.*, 2021, **223**, 2100327.
26 N. Soontornnon, Y. Kimata and Y. Tominaga, *Batteries*, 2022, **8**, 273.
27 N. Soontornnon, K. Kimura and Y. Tominaga, *ACS Appl. Energy Mater.*, 2024, **7**, 4190–4199.
28 H. Aydın and A. Bozkurt, *J. Appl. Polym. Sci.*, 2011, **124**, 1193–1199.
29 X. Cai, Z. Cai, H. Yuan, W. Zhang, S. Wang, H. Wang, J. Lan, Y. Yu and X. Yang, *J. Colloid Interface Sci.*, 2023, **648**, 972–982.
30 A. T. Cruz, G. G. Silva, P. P. D. Souza, T. Matencio, J.-M. Pernaut and M.-A. D. Paoli, *Solid State Ionics*, 2003, **159**, 301–311.
31 M. S. Grewal, M. Tanaka and H. Kawakami, *Polym. Int.*, 2019, **68**, 684–693.
32 Y. L. N. K. Mallela, S. Kim, G. Seo, J. W. Kim, S. Kumar, J. Lee and J.-S. Lee, *Electrochim. Acta*, 2020, **362**, 137141.
33 L. Gu, Y. Gao, Y. Qin, X. Chen, X. Wang and F. Wang, *J. Polym. Sci., Part A: Polym. Chem.*, 2012, **51**, 282–289.
34 I. Kim, J.-T. Ahn, C. S. Ha, C. S. Yang and I. Park, *Polymer*, 2003, **44**, 3417–3428.
35 S. Chen, Z. Hua, Z. Fang and G. Qi, *Polymer*, 2004, **45**, 6519–6524.
36 J. Sebastian and S. Darbha, *RSC Adv.*, 2015, **5**, 18196–18203.
37 C.-S. Tan, C.-C. Juan and T.-W. Kuo, *Polymer*, 2004, **45**, 1805–1814.

38 K. P. Barteau, M. Wolffs, N. A. Lynd, G. H. Fredrickson, E. J. Kramer and C. J. Hawker, *Macromolecules*, 2013, **46**, 8988–8994.
39 X. H. Li, Y. Z. Meng, Q. Zhu and S. C. Tjong, *Polym. Degrad. Stab.*, 2003, **81**, 157–165.
40 S. Peng, Y. An, C. Chen, B. Fei, Y. Zhuang and L. Dong, *Polym. Degrad. Stab.*, 2003, **80**, 141–147.
41 W. Zhu, C. Li, D. Zhang, G. Guan, Y. Xiao and L. Zheng, *Polym. Degrad. Stab.*, 2012, **97**, 1589–1595.
42 B. Sun, J. Mindemark, K. Edström and D. Brandell, *Solid State Ionics*, 2014, **262**, 738–742.
43 Y. Tominaga and K. Yamazaki, *Chem. Commun.*, 2014, **50**, 4448–4450.
44 M. Kerner, N. Plylahan, J. Scheers and P. Johansson, *RSC Adv.*, 2016, **6**, 23327–23334.
45 D. Meghnani, H. Gupta, S. K. Singh, N. Srivastava, R. Mishra, R. K. Tiwari, A. Patel, A. Tiwari and R. K. Singh, *Ionics*, 2020, **26**, 4835–4851.
46 F. Xu, S. Deng, Q. Guo, D. Zhou and X. Yao, *Small Methods*, 2021, **5**, e2100262.
47 Y. Yamada, C. H. Chiang, K. Sodeyama, J. Wang, Y. Tateyama and A. Yamada, *ChemElectroChem*, 2015, **2**, 1687–1694.
48 Y. Yamada, K. Furukawa, K. Sodeyama, K. Kikuchi, M. Yaegashi, Y. Tateyama and A. Yamada, *J. Am. Chem. Soc.*, 2014, **136**, 5039–5046.
49 L. Seidl, R. Grissa, L. Zhang, S. Trabesinger and C. Battaglia, *Adv. Mater. Interfaces*, 2021, **9**, 2100704.
50 K. Kimura, J. Motomatsu and Y. Tominaga, *J. Phys. Chem. C*, 2016, **120**, 12385–12391.
51 Y. Tominaga, K. Nakano and T. Morioka, *Electrochim. Acta*, 2019, **312**, 342–348.
52 L. Li, S. Zhou, H. Han, H. Li, J. Nie, M. Armand, Z. Zhou and X. Huang, *J. Electrochem. Soc.*, 2011, **158**, A74.
53 S. I. Abdul Halim, C. H. Chan and J. Apotheker, *Chemistry Teacher International*, 2021, **3**, 105–115.
54 K. Ariyoshi, A. Mineshige, M. Takeno, T. Fukutsuka, T. Abe, S. Uchida and Z. Siroma, *Electrochemistry*, 2022, **90**, 102008.
55 S. Seki, Y. Kobayashi, H. Miyashiro, Y. Mita and T. Iwahori, *Chem. Mater.*, 2005, **17**, 2041–2045.
56 F. Kaneko, S. Wada, M. Nakayama, M. Wakihara, J. Koki and S. Kuroki, *Adv. Funct. Mater.*, 2009, **19**, 918–925.
57 D. Xiao, Q. Li, D. Luo, G. Li, H. Liu, L. Shui, S. Gourley, G. Zhou, X. Wang and Z. Chen, *Small*, 2020, **16**, e2004688.
58 C. Koga, S. Wada and M. Nakayama, *Electrochim. Acta*, 2010, **55**, 2561–2566.
59 H. Zheng, L. Chai, X. Song and V. Battaglia, *Electrochim. Acta*, 2012, **62**, 256–262.